

PROXT2I: Efficient Reward-Guided Text-to-Image Generation via Proximal Diffusion

Zhenghan Fang
 Johns Hopkins University
 zfang23@jhu.edu

Xiaofeng Gao
 Amazon
 gxiaofen@amazon.com

Jian Zheng
 Amazon
 nzhengji@amazon.com

Jeremias Sulam
 Johns Hopkins University
 jsulam1@jhu.edu

Qiaozi Gao
 Amazon
 qzgao@amazon.com

Abstract

Diffusion models have emerged as a dominant paradigm for generative modeling across a wide range of domains, including prompt-conditional generation. The vast majority of samplers, however, rely on forward discretization of the reverse diffusion process and use score functions that are learned from data. Such forward and explicit discretizations can be slow and unstable, requiring a large number of sampling steps to produce good-quality samples. In this work we develop a text-to-image (T2I) diffusion model based on *backward* discretizations, dubbed PROXT2I, relying on learned and conditional proximal operators instead of score functions. We further leverage recent advances in reinforcement learning and policy optimization to optimize our samplers for task-specific rewards. Additionally, we develop a new large-scale and open-source dataset comprising 15 million high-quality human images with fine-grained captions, called LAION-FACE-T2I-15M, for training and evaluation. Our approach consistently enhances sampling efficiency and human-preference alignment compared to score-based baselines, and achieves results on par with existing state-of-the-art and open-source text-to-image models while requiring lower compute and smaller model size, offering a lightweight yet performant solution for human text-to-image generation.

1 Introduction

Generative artificial intelligence has rapidly transformed the landscape of content creation, enabling the synthesis of realistic text, images, audio, and video. In particular, diffusion models, generative models based on discretizations of stochastic differential equations (SDEs) and ordinary differential equations (ODEs), have emerged as the workhorse behind recent advances in image and text-to-image (T2I) generation (Ho et al., 2020; Song et al., 2021b). By simulating a carefully-designed continuous-time dynamics that transforms noise into data, these diffusion-based methods achieve state-of-the-art image quality and flexible semantic controllability, underpinning many widely used systems such as Stable Diffusion (Rombach et al., 2022), Imagen (Saharia et al., 2022), and DALL·E 2 (Ramesh et al., 2022).

Despite the success of diffusion models, high-quality generation with very few sampling steps remains an open challenge. Conventional score-based samplers, based on forward, explicit discretization of continuous-time processes, often deteriorate significantly in sample quality when the number of steps is reduced, or require carefully tuned and specialized solvers to improve sampling speed (Salimans and Ho, 2022; Lu et al., 2022, 2025). This leads to inefficiencies in practical deployments where fast inference is essential. Efficient sampling is particularly challenging in *human*

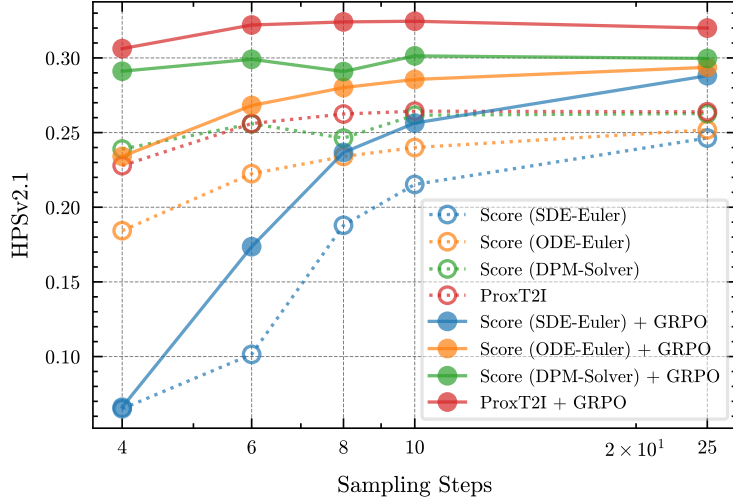


Figure 1: HPSv2.1 score (Wu et al., 2023) vs. number of sampling steps at 256^2 resolution. Our ProxT2I achieves more efficient and human-preference-aligned T2I generation than competing methods.

image generation, where the image quality—particularly for faces and hands—remains less satisfactory, with subtle but very perceptible artifacts or unrealistic features still common (Liao et al., 2024).

An alternative approach to designing diffusion models, recently proposed by (Fang et al., 2025), relies on applying a *backward* discretization to the reverse diffusion process. Unlike traditional forward-discretized solvers that approximate the reverse-time SDE via explicit updates based on scores, the proximal diffusion models from (Fang et al., 2025) employ backward and implicit updates, and leverage proximal operators—instead of the gradients—of the log-density. These proximal-based solvers achieve improved theoretical convergence rates and superior empirical sampling efficiency in generating high-quality samples. So far, proximal diffusion models have been limited to unconditional generation and showcased on low-dimensional data, leaving its potential for conditional generation of high-resolution images unexplored.

Moreover, diffusion models trained simply with denoising score-matching objectives often fall short on downstream objectives such as text-image alignment, aesthetics, safety requirements, or human preference. In this context, reinforcement learning (RL) has become a crucial post-training paradigm to optimize diffusion models for such goals (Black et al., 2024; Fan et al., 2023; Clark et al., 2023; Uehara et al., 2024b,a). Unfortunately, policy-gradient methods in RL typically rely on stochastic sampling paths and are therefore not directly applicable to deterministic (and faster) ODE-based samplers, necessitating ad hoc modifications (Liu et al., 2025; Xue et al., 2025). In contrast, proximal diffusion provides an efficient yet stochastic SDE-based sampler with speed comparable to ODE methods (Fang et al., 2025), making it naturally amenable to RL. Yet, the distinct non-Gaussian transition kernel in proximal-based samplers introduces challenges for applying RL objectives, which are defined using transition densities. This motivates the main question in this work: *Can we combine the improved speed of proximal diffusion models with the flexibility of reinforcement learning to optimize task-specific rewards in T2I generation?*

We answer this question positively by introducing PROXT2I, a text-conditional proximal diffusion model augmented with reinforcement learning for T2I generation. More specifically, our contributions are:

1. We leverage the proximal diffusion framework (Fang et al., 2025) to develop a new conditional generative model for efficient, high-quality human text-to-image synthesis.
2. We integrate reinforcement learning via Group Relative Policy Optimization (GRPO) (Shao et al., 2024) into proximal diffusion, improving perceptual quality and text-image alignment while preserving the fast sampling advantages of proximal-based samplers.
3. We curate and opensource **LAION-Face-T2I-15M**, a new large-scale dataset of 15M high-quality human images with fine-grained captions and a 3M hand-focused subset, establishing a new foundation for developing human T2I models.
4. As will be demonstrated, PROXT2I offers a lightweight and efficient solution for fine-grained, text-conditional human image generation with state-of-the-art performance.

The rest of the paper is organized as follows. Section 2 introduces related works on diffusion models, text-to-image generation, and reinforcement learning. Section 3 then presents the proposed approach, while our experiments and results are presented in Section 4. Discussion of limitations and conclusion are finally addressed in Section 5.

2 Related Works

Diffusion Models. Diffusion models have emerged as one of the most popular frameworks for generative modeling, offering a principled way to learn and sample from complex data distributions through iterative denoising (Sohl-Dickstein et al., 2015; Ho et al., 2020; Song et al., 2021b). Diffusion models sample data by simulating the reverse of a forward noising process (Song et al., 2021b), where the reverse-time dynamics are governed by an SDE (or its deterministic ODE counterpart). Sampling then amounts to discretizing this reverse process, typically using explicit solvers analogous to Euler–Maruyama schemes, resulting in updates that invoke the gradient of the log-density (*a.k.a.* the score) at each step (Song et al., 2021b). Compared to conventional approaches such as VAEs or GANs, diffusion models are favored for their training stability, high sample quality, and natural flexibility to conditional generation through mechanisms like classifier-free guidance (Dhariwal and Nichol, 2021; Ho and Salimans, 2022). However, these advantages come at the cost of computational inefficiency, as explicit, forward discretizations of the reverse process typically require a large number of small sampling steps to ensure good sample fidelity, and score-based updates can be sensitive to hyperparameter choice and lack of regularity in the data distribution (Karras et al., 2022; Chen et al., 2023; Beyler and Bach, 2025). *Proximal Diffusion Models (ProxDMD)* (Fang et al., 2025) offer an alternative formulation by applying a *backward discretization* to the reverse SDE, casting each update as an implicit step that defines a proximal operator of the log-density of the data distribution (see more details in Section 3). This enhances stability and allows considerably larger step sizes and faster convergence, providing a principled and efficient foundation for generative sampling.

Diffusion models and reinforcement learning for T2I generation. Diffusion models have achieved remarkable success in text-to-image generation with power approaches such as Stable Diffusion (Rombach et al., 2022), Imagen (Saharia et al., 2022), and DALL·E 2 (Ramesh et al., 2022). However, as with unconstrained sampling, these methods require many sampling steps to achieve high quality. Considerable work has focused on accelerating inference through ODE-based samplers and flow-matching models (Song et al., 2021a; Lipman et al., 2022; Lu et al., 2022), or via knowledge distillation (Salimans and Ho, 2022; Luhman and Luhman, 2021; Chen et al., 2025).

Despite these advances, few-step samplers often require additional distillation training or suffer from degraded fidelity or limited robustness. Beyond conventional pretraining on data samples, reinforcement learning (RL) has been explored to directly align generative models with downstream objectives or human preferences (Black et al., 2024; Liu et al., 2025; Xue et al., 2025; Hu et al., 2025). GRPO-based approaches in particular improve stability and scalability but often rely on modified versions of deterministic flow-based samplers with added noise for stochastic exploration (Liu et al., 2025; Xue et al., 2025). Our work will instead leverage the intrinsic stochasticity of proximal diffusion, enabling a natural integration with GRPO for efficient, reward-guided text-to-image generation.

3 Methods

We now first introduce some background on diffusion models, laying the necessary elements for PROXT2I. We will then introduce our conditional proximal diffusion model, and demonstrate how a proximal variant of classifier-free guidance (Ho and Salimans, 2021) can be applied to flexibly control the conditioning strength and improve image quality. Finally, we will describe how RL, and the GRPO algorithm in particular, can be incorporated with proximal sampling for task-specific reward optimization.

3.1 Warm-up: Proximal Diffusion Models

Diffusion models are built upon reversing a stochastic forward process that progressively perturbs data toward a simple and known distribution, typically a standard Gaussian. A common choice for this is the Ornstein–Uhlenbeck (OU) process, described by the following SDE:

$$dX_t = -\frac{1}{2}X_t dt + dW_t, \quad t \in [0, T],$$

where $X_t \in \mathbb{R}^d$ denotes the sample at time t and $W_t \in \mathbb{R}^d$ is a standard Wiener process (i.e., Brownian motion). Here, $X_0 \sim p_{\text{data}}$ follows the data (target) distribution. It can be shown (Oksendal, 2013) that the marginal distribution of X_t is a mixture of the data distribution and a standard normal with time-evolving weights: $X_t \stackrel{d}{=} \sqrt{e^{-t}}X_0 + \sqrt{1 - e^{-t}}\xi$, $\xi \sim \mathcal{N}(0, I)$. As $T \rightarrow \infty$, the distribution of X_T converges to the standard Gaussian. In practice, it is common to introduce a scheduling function $\beta(t) : \mathbb{R} \rightarrow \mathbb{R}^+$ to control the diffusion rate while fixing $T = 1$:

$$dX_t = -\frac{1}{2}\beta(t)X_t dt + \sqrt{\beta(t)}dW_t, \quad t \in [0, 1]. \quad (1)$$

The corresponding marginal distribution satisfies $X_t \stackrel{d}{=} \sqrt{\alpha_t}X_0 + \sqrt{1 - \alpha_t}\xi$, $\xi \sim \mathcal{N}(0, I)$, where $\alpha_t = \exp(-\int_0^t \beta(s)ds)$. A commonly used choice is a linear schedule: $\beta(t) = \beta_{\min} + (\beta_{\max} - \beta_{\min})t$.

The generative process reverses the forward one by simulating the reverse-time SDE (Anderson, 1982; Song et al., 2021b):

$$dX_t = \left[-\frac{1}{2}\beta(t)X_t - \beta(t)\nabla \ln p_t(X_t) \right] dt + \sqrt{\beta(t)}d\bar{W}_t,$$

where \bar{W}_t denotes a reverse-time Wiener process. This SDE preserves the marginal distributions of (1) (Anderson, 1982), and thus one can approximate samples from p_{data} by drawing $X_{t=1} \sim \mathcal{N}(0, I)$ and then numerically integrating the reverse-time SDE from $t = 1$ to $t = 0$.

To make this approach practical, the reverse-time SDE must be discretized and integrated using numerical solvers. A standard choice is the forward discretization, i.e., the explicit Euler–Maruyama scheme:

$$X_{k-1} = X_k + \gamma_k \left[\frac{1}{2} X_k + \nabla \ln p_{t_k}(X_k) \right] + \sqrt{\gamma_k} \xi_k, \quad (2)$$

where X_k and X_{k-1} represent the current and next iterates, respectively, $\xi_k \sim \mathcal{N}(0, I)$ and $\gamma_k = \beta(t_k)(t_{k-1} - t_k)$ is the step size scaled by $\beta(t)$. In practice, the true score function $\nabla \ln p_t(X_t)$ is approximated by a trained neural network $s_\theta(X_t, t)$, resulting in score-based diffusion models. This explicit discretization scheme underlies the vast majority of diffusion samplers, including standard (Ho et al., 2020; Song et al., 2021b) and accelerated ones (Song et al., 2021a; Zhang and Chen, 2023; Lu et al., 2022; Wu et al., 2024; Lu et al., 2025).

Proximal Diffusion Models. An alternative approach to score-based solvers is to apply *backward discretization*:

$$X_{k-1} = X_k + \gamma_k \left[\frac{1}{2} X_{k-1} + \nabla \ln p_{t_{k-1}}(X_{k-1}) \right] + \sqrt{\gamma_k} \xi_k,$$

where the drift term is evaluated at the next iterate (note the dependence on X_{k-1} on the right-hand side). Although the update rule for the next iterate X_{k-1} now becomes implicit, this implicit equation can be expressed explicitly using a *proximal operator* (Fang et al., 2025). For a scalar-valued (and weakly-convex) function $f: \mathbb{R}^d \rightarrow \mathbb{R}$, its proximal operator is a mapping from \mathbb{R}^d to \mathbb{R}^d defined as

$$\text{prox}_f(x) = \arg \min_u f(u) + \frac{1}{2} \|u - x\|_2^2,$$

which intuitively finds a point u that approximately minimizes f while remaining close to x . To see its connection with backward discretization, we can apply the first-order optimality conditions¹ and obtain the following property:

$$\nabla f(\text{prox}_f(x)) + \text{prox}_f(x) - x = 0, \quad (3)$$

indicating that $y = \text{prox}_f(x)$ is a solution to the implicit equation $\nabla f(y) + y - x = 0$. Thus, by re-arranging the backward-discretized update, one can obtain the *proximal diffusion algorithm* (PDA) from (Fang et al., 2025),

$$X_{k-1} = \text{prox}_{\frac{2\gamma_k}{2-\gamma_k} \ln p_{t_{k-1}}} \left(\frac{2}{2-\gamma_k} (X_k + \sqrt{\gamma_k} \xi_k) \right).$$

However, this algorithm requires $\gamma_k < 2$ to maintain positive coefficients, imposing a hard constraint on the maximum step size possible. This restriction can be relaxed using the alternative *hybrid scheme*, which incorporates both forward and backward discretizations:

$$X_{k-1} = X_k + \gamma_k \left[\frac{1}{2} X_k + \nabla \ln p_{t_{k-1}}(X_{k-1}) \right] + \sqrt{\gamma_k} \xi_k,$$

yielding the *hybrid proximal diffusion algorithm* (PDA-hybrid):

$$X_{k-1} = \text{prox}_{-\gamma_k \ln p_{t_{k-1}}} \left[(1 + \frac{1}{2} \gamma_k) X_k + \sqrt{\gamma_k} \xi_k \right]. \quad (4)$$

¹We assume f to be smooth for simplicity of presentation, though this is not necessary.

This formulation lifts the step-size restriction and remains valid at large γ_k .

Importantly, the proximal operators in these algorithms can be learned directly from data via proximal matching (Fang et al., 2024), analogous to score matching for score-based models, thereby enabling *generative modeling*. These proximal diffusion models exhibit theoretically improved iteration complexity compared to forward-discretized, score-based samplers (Chen et al., 2023; Benton et al., 2024) and achieve empirically faster inference in generating high-quality images (Fang et al., 2025). Moreover, because proximal diffusion models rely on SDE discretization, they intrinsically incorporate stochasticity in the sampling trajectory (through the terms ξ_k). As we shall see shortly, this property makes PDA and PDA-hybrid particularly amenable to reinforcement learning, which relies on stochasticity in the sampling process for exploration (which is not satisfied by the sampling paths of probability-flow ODEs (Song et al., 2021a,b; Zhang and Chen, 2023; Lu et al., 2022) or flow matching models (Lipman et al., 2022; Liu et al., 2023)).

In the following sections, we will extend PDA(-hybrid) to conditional generation and show how to integrate them with GRPO to optimize for task-specific reward models.

3.2 Proximal Diffusion for Conditional Generation

Conditional generation is concerned with drawing samples from the conditional distribution of $p_{\text{data}}(\cdot | c)$, where $c \in \mathbb{R}^{d_c}$ is a conditioning signal, e.g. the embedding of some input text in T2I generation. The forward process for conditional sampling is defined analogously to the unconditional case (1), but initialized at the conditional data distribution: $X_0 \sim p_{\text{data}}(\cdot | c)$. This conditional forward process admits the following reverse-time SDE:

$$dX_t = \left[-\frac{1}{2}\beta(t)X_t - \beta(t)\nabla \ln p_t(X_t | c) \right] dt + \sqrt{\beta(t)} d\bar{W}_t, \quad (5)$$

where $\nabla \ln p_t(\cdot | c)$ is the score of the data distribution of the conditional forward process at time t . To sample from $p_{\text{data}}(\cdot | c)$, score-based samplers discretize Eq. (5) using a forward Euler scheme while parameterizing the conditional score at each step with a neural network that takes c as an additional input. In contrast, in this work we leverage the hybrid discretization from PDA-hybrid to integrate Eq. (5):

$$X_{k-1} = X_k + \frac{1}{2}\gamma_k \left[X_k + \nabla \ln p_{t_{k-1}}(X_{k-1} | c) \right] + \sqrt{\gamma_k} \xi_k,$$

which can be rewritten as:

$$X_{k-1} = \text{prox}_{-\gamma_k \ln p_{t_{k-1}}(\cdot | c)} \left[(1 + \frac{1}{2}\gamma_k)X_k + \sqrt{\gamma_k} \xi_k \right], \quad (6)$$

by the first-order optimality condition of the proximal. Each iteration thus evaluates the proximal operator of the *conditional* log-density $\ln p_{t_{k-1}}(\cdot | c)$, guiding samples toward high-likelihood regions of the conditional data distribution.

Although the vanilla algorithm in Eq. (6) can in principle achieve conditional generation, in practice it often produces samples with suboptimal quality and weak coherence to the conditioning signal, as also observed in score-based models (Ho and Salimans, 2021; Rombach et al., 2022). A widely adopted solution in popular text-to-image models (Nichol et al., 2021; Rombach et al., 2022; Podell et al., 2024; Esser et al., 2024) is *classifier-free guidance* (CFG) (Ho and Salimans, 2021, 2022), which strengthens the conditional signal by linearly combining the conditional and unconditional scores. Inspired by this approach, we introduce a proximal variant of the CFG technique:

$$X_{k-1} = f_\omega \left[(1 + \frac{1}{2}\gamma_k)X_k + \sqrt{\gamma_k} \xi_k; c \right] \quad (7)$$

by using the linear combination of conditional and unconditional proximal mappings:

$$f_\omega(x; c) = (1 + \omega) \operatorname{prox}_{-\gamma_k \ln p_{t_{k-1}}(\cdot | c)}(x) \\ - \omega \operatorname{prox}_{-\gamma_k \ln p_{t_{k-1}}}(x).$$

When $\omega = 0$, this reduces to the standard conditional proximal update in Eq. (6), while for $\omega > 0$, the update direction is amplified by the discrepancy between the conditional and unconditional proximal mappings—thereby steering each step toward regions favored by the conditioning signal and away from the unconditional samples. Analogous to score models, larger ω values encourage stronger semantic alignment with the conditioning input c . As we will demonstrate in our experiments, this guidance mechanism substantially enhances the sample fidelity and conditioning consistency of the proximal diffusion sampler while maintaining its high sampling efficiency.

Learning Conditional Proximal Functions. To achieve generative modeling using the sampling scheme above, the time-specific proximal operators of the log-density must be learned from data. We consider a neural network $f_\theta(x; t, \lambda, c)$ that parameterizes the conditional proximal operator $\operatorname{prox}_{-\lambda \ln p_t(\cdot | c)}(x)$, and our goal is to train f_θ for all possible $\{t, \lambda, c\}$ tuples. Similar to the unconditional proximal models, we train these conditional proximals using the *proximal matching* objective from Fang et al. (2024), which resembles denoising score matching but replaces the mean squared error with a specialized loss that encourages approximation of the mode of a conditional distribution—coinciding with the interpretation of proximal operators as the Maximum A Posteriori (MAP) denoiser under Gaussian noise. To train these operators, we minimize the following loss:

$$\mathcal{L}(\theta) = \mathbb{E}_{t, \lambda, c, X_t, \varepsilon} \left\{ \ell_{\text{PM}} \left[f_\theta(X_t + \sqrt{\lambda} \varepsilon; t, \lambda, c), X_t; \zeta \right] \right\} \quad (8)$$

where (t, λ) is drawn from a predefined distribution $p(t, \lambda)$, $X_t \sim p_t(\cdot | c)$ is sampled from the forward process at time t (conditioned on c), and $\varepsilon \sim \mathcal{N}(0, I)$ is standard Gaussian noise. Importantly,

$$\ell_{\text{PM}}(x, y; \zeta) = 1 - \exp \left(-\frac{\|x - y\|_2^2}{d\zeta^2} \right)$$

is the proximal matching loss (Fang et al., 2024), where $\zeta \in \mathbb{R}^+$ is a hyperparameter that balances the approximation error to the proximal and the smoothness of the loss function. It can be shown that the minimizer of Eq. (8), $f_{\theta^*}(x; t, \lambda, c)$, approaches the desired proximal operator, $\operatorname{prox}_{-\lambda \ln p_t(\cdot | c)}(x)$, as $\zeta \rightarrow 0$.

To support the CFG technique, we will also need to learn the unconditional proximal operator $\operatorname{prox}_{-\lambda \ln p_t}(x)$. Following standard practice (Ho and Salimans, 2022), we parameterize both the unconditional and conditional proximal functions using a single neural network, and set the input condition c to a null context \emptyset for evaluating the unconditional model. In text-to-image generation, this corresponds to using the embedding of an empty text as c . To train the unconditional model, we simply replace c with \emptyset in each training sample (X_t, c) following a predefined probability p_\emptyset (we let $p_\emptyset = 0.1$ following prior work (Bao et al., 2023)). This design effectively enables the network to learn the proximal operators of both the conditional and unconditional log-densities.

3.3 Proximal Diffusion Policy Optimization

The conditional proximal diffusion described above already enables sampling from the desired conditional distribution. Indeed, in the idealized limit of infinite training data (and compute),

infinite network capacity, and an unlimited budget of sampling steps, it would generate samples that match the data distribution. However, beyond faithfully matching a data distribution, many use cases of generative models are more concerned with task-specific, downstream objectives, such as human-perceived quality and prompt-image alignment (Black et al., 2024). We will now show how to apply reinforcement learning to directly optimize our proximal models for such objectives.

Consider a Markov decision process (MDP) whose rounds are indexed by k , with state s_k , action a_k , reward $R(s_k, a_k)$, and policy π_θ . The goal of reinforcement learning is to learn a policy that maximizes the expected time-cumulative reward over sampled trajectories:

$$\max_{\theta} \mathbb{E}_{(s_0, a_0, \dots, s_K, a_K) \sim \pi_\theta} \left[\sum_{k=0}^K R(s_k, a_k) \right].$$

To apply these ideas to diffusion models, the sampling procedure is typically mapped to an MDP (Black et al., 2024), where the state is a tuple of conditioning, step index, and the current sample: $s_k \triangleq (c, k, X_k)$, the action is the next sample $a_k \triangleq X_{k-1}$, and the policy is the corresponding transition kernel $\pi_\theta(a_k | s_k) \triangleq p_\theta(X_{k-1} | X_k, c)$, describing how the sample evolves from step k to $k-1$. To optimize this policy, we adopt Group Relative Policy Optimization (GRPO) (Shao et al., 2024), a lightweight and scalable variant of Proximal Policy Optimization (PPO) (Schulman et al., 2017) that has been successfully applied to text-to-image flow models (Liu et al., 2025). For each conditioning c , GRPO first samples a group of trajectories $\{\tau^{(i)}\}_{i=1}^G$, with $\tau^{(i)} = (X_K^{(i)}, X_{K-1}^{(i)}, \dots, X_0^{(i)})$. The final outputs $\{X_0^{(i)}\}$ are evaluated by a reward function $R(X_0^{(i)}, c)$, and the *group-relative advantages* are then computed by:

$$\hat{A}^{(i)} = \frac{R(X_0^{(i)}, c) - \text{mean}(\{R(X_0^{(i)}, c)\}_{i=1}^G)}{\text{std}(\{R(X_0^{(i)}, c)\}_{i=1}^G)}.$$

Such a formulation aligns with the comparative nature of most reward models and provides a more stable and informative signal for policy optimization (Shao et al., 2024). To use these computed advantage to perform policy optimization, we can maximize the following objective²:

$$\mathcal{J}_{\text{GRPO}}(\theta) = \sum_{i=1}^G \sum_{k=1}^K \left\{ R_k^{(i)}(\theta) - \beta_{\text{KL}} D_{\text{KL}, k}^{(i)}(\theta) \right\},$$

where

$$R_k^{(i)}(\theta) = \frac{p_\theta(X_{k-1}^{(i)} | X_k^{(i)}, c)}{p_{\theta_{\text{old}}}(X_{k-1}^{(i)} | X_k^{(i)}, c)} \hat{A}^{(i)},$$

with θ_{old} denoting the parameters before the current update step. Intuitively, the objective encourages the model to assign higher probability to the samples $X_{k-1}^{(i)}$ from paths with positive advantages, while penalizing those with negative ones. The KL regularization term

$$D_{\text{KL}, k}^{(i)}(\theta) = \text{KL} \left[p_\theta(\cdot | X_k^{(i)}) \parallel p_{\theta_{\text{ref}}}(\cdot | X_k^{(i)}) \right]$$

prevents the policy from drifting too far from a fixed reference model θ_{ref} , typically set as the pre-trained model before reinforcement learning, and $\beta_{\text{KL}} \in \mathbb{R}^+$ controls the strength of regularization. As the objective shows, optimizing θ hinges on evaluation of the transition kernel $p_\theta(X_{k-1}^{(i)} | X_k^{(i)}, c)$ and its gradient with respect to θ – which we derive next.

²Here we present a simplified version of the GRPO objective for simplicity of presentation. The full definition can be found in Section A.

Integrating RL with proximal diffusion. For score-based diffusion models, the transition kernel $p_\theta(X_{k-1} | X_k, c)$ is Gaussian (Black et al., 2024) and permits efficient evaluation of the GRPO objective. Nonetheless, the transition kernel corresponding to the proximal diffusion update (Eq. (7)) is:

$$p_\theta(X_{k-1} | X_k, c) = [f_\omega(\cdot; c)]_\# \mathcal{N}((1 + \frac{1}{2}\gamma_k)X_k, \gamma_k I),$$

where $h_\#$ denotes the pushforward of a distribution under the mapping h . Equivalently, X_{k-1} is given by pushing forward a Gaussian through the deterministic mapping $f_\omega(\cdot; c)$, a linear combination of conditional and unconditional proximal networks. This results in a *non-Gaussian* transition kernel that is, in general, intractable to evaluate. Only under strong assumptions, such as when f_ω is invertible, one can leverage change-of-variables to obtain an analytical expression for the ratio of kernels. However, since the proximal networks in our formulation are not constrained to be bijective or have tractable Jacobian determinants, direct computation of p_θ remains infeasible.

To address this issue, we introduce an auxiliary variable that yields tractable Gaussian transitions. Let

$$Y_k = (1 + \frac{1}{2}\gamma_k)X_k + \sqrt{\gamma_k} \xi_k, \quad k = 1, \dots, K. \quad (9)$$

and $Y_0 = X_0$. Then, the sampling process in (7) can be rewritten as

$$\begin{aligned} Y_K &\sim \mathcal{N}(0, [(1 + \frac{1}{2}\gamma_K)^2 + \gamma_K]I), \\ Y_{k-1} &= (1 + \frac{1}{2}\gamma_{k-1})f_\omega(Y_k; c) + \sqrt{\gamma_{k-1}}\xi_{k-1}, \quad k = K, \dots, 2, \\ Y_0 &= f_\omega(Y_1; c), \end{aligned}$$

and the resulting variables $\{Y_k\}_{k=0}^K$ now admit explicit Gaussian transition kernels:

$$p_\theta(Y_{k-1} | Y_k, c) = \mathcal{N}((1 + \frac{1}{2}\gamma_{k-1})f_\omega(Y_k; c), \gamma_{k-1}I),$$

for $k = K, \dots, 2^3$. Under this new formulation, the GRPO objective can be directly applied to the proximal sampler through the MDP defined by $\{Y_k\}_{k=0}^K$, enabling tractable evaluation of the GRPO objective in the proximal setting.

The application of RL to generative models based on efficient ODE and flow-based samplers often requires careful modifications of the sampling process to inject stochasticity necessary for exploration (Liu et al., 2025; Xue et al., 2025). In contrast, proximal diffusion models provide comparable sampling efficiency to ODE-based samplers while retaining the stochasticity from SDE discretization, allowing direct application of RL without modification of the sampling path. Notably, the efficiency and stochasticity of proximal sampling could also be useful in other methods that require random transitions, such as inference-time reward alignment (Holderrieth et al., 2025).

3.4 LAION-Face-T2I-15M Dataset

Although text-to-image generation models have achieved remarkable progress, finegrained generation of human features (such as hands and faces) remains a major challenge. While methods keep evolving, existing open datasets are either limited in scale, domain-specific (e.g., face-only), or lack comprehensive and rich textual descriptions (Xia et al., 2021a,b; Ju et al., 2023; Li et al., 2024). Thus, in this work we also curate, collect, and opensource LAION-FACE-T2I-15M, a dataset of 15M text-image pairs designed for human-domain text-to-image generation. LAION-Face-T2I-15M

³We use \mathcal{N} to denote the density of a Gaussian.

builds upon LAION-Face⁴, a filtered subset of LAION-400M curated to contain high-quality images with human faces. We further filter the dataset based on image size and aesthetic score (Schuhmann, 2022), resulting in a high-resolution and high-quality collection of roughly 15M images. To improve the details in caption for fine-grained generation, we recaption all images using the Qwen-2.5-7B vision-language model (Qwen et al., 2025) with a carefully-designed prompt that promotes accurate, comprehensive, and fine-grained textual descriptions. The resulting captions describe not only facial attributes but also hair, makeup, clothing, ethnicity⁵, image background and overall image style (e.g., photography vs. artwork). This process yields high-quality captions suitable for training human text-to-image models from scratch. Additionally, we also construct LAION-Face-Hand-3M, a subset of LAION-Face-T2I-15M tailored for hand image generation. We employ Qwen-2.5-7B with a dedicated prompt to identify images containing close-up views of hands and generate detailed captions describing the hand attributes. This results in approximately 3M images containing human hands paired with descriptive captions that describe the number of hands, their position relative to the body, finger gestures, interactions (e.g., holding objects or touching the face), and visibility quality. This provides valuable data for learning human-hand generation, an area where current models often fail.

We will publicly release LAION-Face-T2I-15M and LAION-Face-Hand-3M, including all generated captions and image URLs, upon publication of this paper. By combining careful filtering, high-quality recaptioning, and targeted hand-focused subsets, we hope this collection of data will serve as a valuable resource for the research community and facilitate the pretraining and finetuning of human-domain text-to-image models. More details on data processing, including detailed prompts, can be found in Section B. Examples from the dataset are provided in Fig. 5.

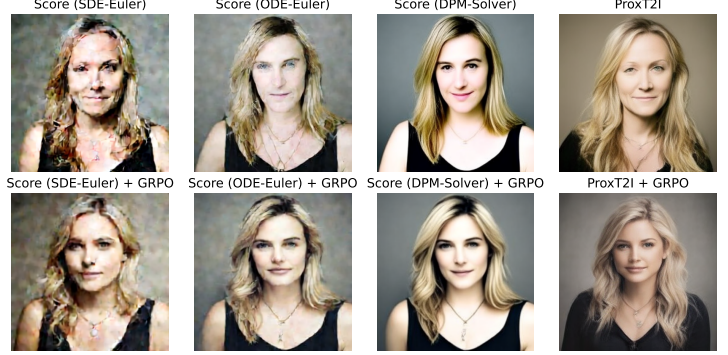
4 Experiments and Results

We perform generation in the latent space of a variational autoencoder (VAE) (Rombach et al., 2022; Esser et al., 2024) and use a combination of text encoders (MetaCLIP (Xu et al., 2023a) and T5 (Raffel et al., 2020)) for textual embedding. The U-ViT network (Bao et al., 2023) is adopted as the backbone for both proximal and competing score networks for its flexibility in handling varying input dimensions. All models are trained from scratch on the LAION-Face-T2I-15M dataset and subsequently finetuned with GRPO. More experimental details can be found in Section C.

We compare against multiple score-based samplers: 1) “SDE-Euler” employs the standard Euler-Maruyama discretization on the reverse-time SDE in Eq. (5); 2) “ODE-Euler” applies Euler discretization to the probability flow ODE (Song et al., 2021b); and 3) “DPM-solver” is the fast higher-order solver proposed in (Lu et al., 2022). Note that only the SDE-Euler is a “fair” comparison model (since ProxT2I also discretizes an SDE) but, as we will see, ProxT2I also outperforms ODE and DPM solvers. We use CFG with $\omega = 4$ for all the models. To facilitate quantitative comparison, we compute four metrics estimating human preference alignment and aesthetic quality: HPSv2.1 (Wu et al., 2023), Aesthetic score (Schuhmann, 2022), ImageReward (Xu et al., 2023b), and PickScore (Kirstain et al., 2023).

⁴<https://github.com/FacePerceiver/LAION-Face>

⁵Automatically generated captions may be biased or inaccurate in describing perceived ethnicity or gender, and large-scale human datasets can inherit demographic biases from their data sources. Unfortunately, the LAION dataset (from which we derive ours) does not have ground truth demographic attributes, as they are images crawled from the web, and thus no real analysis can be provided. We refer the reader to the recent discussion in (Girrbach et al., 2025) for the LAION dataset, and advise caution when employing any demographic attributes in our dataset.



“A woman with long blonde hair and a black top stands against a neutral background. She wears a delicate necklace. The image is a portrait-style photograph with soft lighting.”

Figure 2: Samples generated by ProxT2I and competing methods at 256^2 resolution using 10 sampling steps.

4.1 Comparison with competing methods

Results at 256^2 Resolution. Fig. 1 presents the HPSv2.1 scores at 256^2 resolution across different samplers and step counts and Fig. 2 visualizes image samples. Fig. 6 in Appendix presents additional samples and Fig. 7 provides additional metrics. Results are averaged over a held-out testing set of 1024 prompts. Among non-RL methods, ProxT2I already outperforms SDE-Euler and ODE-Euler and is competitive with DPM-Solver. When fine-tuned with GRPO, the numerical results of ProxT2I significantly improves, demonstrating the effectiveness of the proposed proximal diffusion policy optimization approach. Among all methods, the improvements from GRPO are most pronounced for ProxT2I. ProxT2I-GRPO consistently outperforms score-based RL-finetuned models and achieves the highest performance across sampling step numbers and metrics, demonstrating efficient and human-preference-aligned T2I generation. Notably, ProxT2I-GRPO also achieves strong results at just 4 sampling steps, despite the fact that RL training was applied to the Markov decision process at 10 sampling steps, demonstrating good generalization ability of RL and sharper and more human-preference-aligned generations even in very low step regimes.

Results at 512^2 Resolution. We further evaluate the models’ performance for high-resolution generation at 512^2 . Fig. 3 presents HPSv2.1 scores and visual samples (additional metrics and samples can be found in Figs. 8 and 9, respectively). Notably, ProxT2I achieves notable improvements over all score-based solvers both before and after RL finetuning, particularly in low-step sampling regimes, demonstrating that the efficiency benefits of ProxT2I scale to higher-dimensions.

Comparison with external open-source models. To evaluate our model’s performance among widely-used text-to-image models, we compare with Stable Diffusion (SD) 3.5 Medium (Esser et al., 2024) and its respective GRPO-fine-tuned variant (Liu et al., 2025), with HPSv2.1 results shown in Figure 4 and additional metrics in Fig. 10. It is important to note that this comparison is not strictly fair: ProxT2I employs a lighter backbone (a transformer with approximately 500 million parameters), and is trained using data and protocols that will be publicly released. In contrast, SD 3.5 uses a substantially larger transformer with about 2.2 *billion* parameters and is trained on a mixture of synthetic and filtered public data, though the specific details on training strategy and dataset are not fully disclosed. Furthermore, SD 3.5 is a general-domain model, while ProxT2I is trained specifically for human image synthesis. Despite these differences, ProxT2I achieves competitive performance relative to SD 3.5, particularly at low sampling steps. These results demonstrate

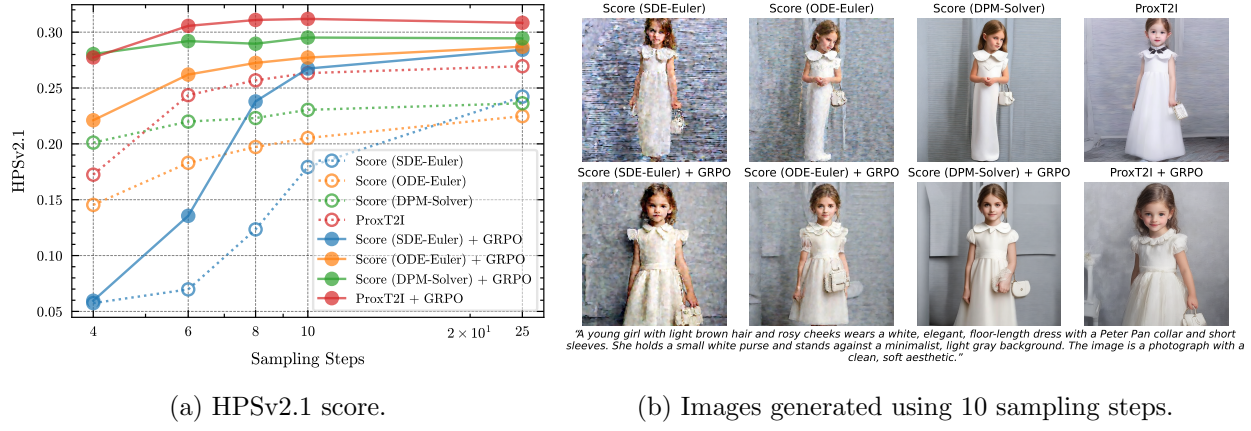


Figure 3: Comparison between ProxT2I and competing methods at 512^2 resolution.

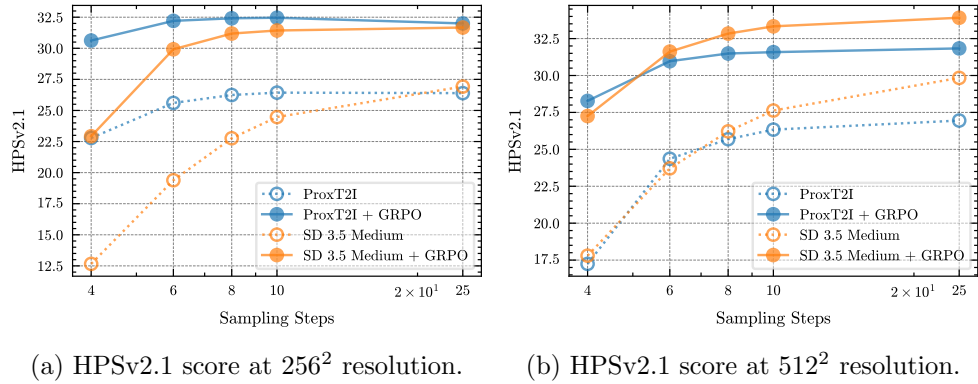


Figure 4: Comparison with Stable Diffusion (SD) 3.5 Medium (Esser et al., 2024) and its Flow-GRPO-finetuned variant (Liu et al., 2025).

that ProxT2I offers a lightweight and efficient solution for human-domain text-to-image generation that requires substantially less compute and memory without significantly degrading generation quality.

4.2 Ablation Studies

Classifier-free guidance. We further study the influence of the classifier-free guidance (CFG) level, ω , in our results. Fig. 11 shows the numerical results at different ω values on 256^2 images over a validation set of 256 prompts (model trained without GRPO), with visual samples shown in Fig. 12. Note that $\omega = 0$ represents the sampler without classifier-free guidance, i.e., using only the conditional proximal operator. It is clear that using CFG ($\omega > 0$) effectively improves image quality, with the performance peaking around $\omega = 4.0$. Note also that this parameter is quite stable as a function of the number of sampling steps.

Ablation of reward models. To study the influence of different reward models in reinforcement learning, we finetune the pretrained ProxT2I model at 256^2 resolution with two other reward functions—ImageReward (Xu et al., 2023b) and Aesthetic score (Schuhmann, 2022)—in addition to PickScore (Kirstain et al., 2023). Fig. 13 demonstrates that training with each reward function leads to a noticeable improvement in its corresponding metric over the pretrained baseline, confirming the

effectiveness of RL fine-tuning for the proximal diffusion model. Among the three, the PickScore reward produces the most consistent improvements across all metrics and achieves the largest gain on the external metric HPSv2.1. The Aesthetic Score reward, while significantly enhancing the result on its own, leads to degradation in all other metrics due to reward hacking: as depicted in Fig. 14, the model initially learns to generate more aesthetically appealing images but eventually collapses, generating virtually identical images for all input prompts.

5 Conclusion and Limitations

We presented ProxT2I(-GRPO), a human-domain text-to-image framework that unifies proximal diffusion models with reinforcement learning. By extending proximal sampling to conditional generation and integrating it with policy optimization, our approach directly addresses the challenges of efficiency, generation quality, and human-preference alignment in few-step T2I generation. We further presented LAION-Face-T2I-15M, a large-scale dataset with fine-grained captions that provides a strong foundation for developing human T2I models. Experiments demonstrate that ProxT2I-GRPO achieves state-of-the-art performance at very low step counts, surpassing score-based samplers and performing competitively with larger open-source systems despite requiring fewer parameters. These results highlight the potential of proximal diffusion models for efficient, high-quality and reward-guided generation.

Our approach has several limitations and potential societal impacts. RL is sensitive to the design of the reward model, which may encode undesired biases from the training data, and optimizing for such signals risks overfitting to spurious correlations rather than true human preference. Human image generation and large-scale human image dataset can also raise ethical concerns related to privacy, consent, and fairness, and models may perpetuate demographic biases in data sources. The lack of ground-truth demographic data in LAION complicates the analysis of this limitation further. Finally, while ProxT2I-GRPO demonstrates strong performance for human-domain T2I, future work will include extending it to broader domains, exploring alternative reward signals for alignment, and scaling to ultra-high resolutions.

References

Brian DO Anderson. Reverse-time diffusion equation models. *Stochastic Processes and their Applications*, 12(3):313–326, 1982.

Fan Bao, Shen Nie, Kaiwen Xue, Yue Cao, Chongxuan Li, Hang Su, and Jun Zhu. All are worth words: A vit backbone for diffusion models. In *Proceedings of the IEEE/CVF conference on computer vision and pattern recognition*, pages 22669–22679, 2023.

Joe Benton, Valentin De Bortoli, Arnaud Doucet, and George Deligiannidis. Nearly $\$d\$$ -linear convergence bounds for diffusion models via stochastic localization. In *The Twelfth International Conference on Learning Representations*, 2024.

Eliot Beyler and Francis Bach. Optimal denoising in score-based generative models: The role of data regularity. *arXiv preprint arXiv:2503.12966*, 2025.

Kevin Black, Michael Janner, Yilun Du, Ilya Kostrikov, and Sergey Levine. Training diffusion models with reinforcement learning. In *The Twelfth International Conference on Learning Representations*, 2024.

Hongrui Chen, Holden Lee, and Jianfeng Lu. Improved analysis of score-based generative modeling: User-friendly bounds under minimal smoothness assumptions. In *International Conference on Machine Learning*, pages 4735–4763. PMLR, 2023.

Tianyu Chen, Yasi Zhang, Zhendong Wang, Ying Nian Wu, Oscar Leong, and Mingyuan Zhou. Denoising score distillation: From noisy diffusion pretraining to one-step high-quality generation. *arXiv preprint arXiv:2503.07578*, 2025.

Kevin Clark, Paul Vicol, Kevin Swersky, and David J Fleet. Directly fine-tuning diffusion models on differentiable rewards. *arXiv preprint arXiv:2309.17400*, 2023.

Prafulla Dhariwal and Alexander Nichol. Diffusion models beat gans on image synthesis. *Advances in neural information processing systems*, 34:8780–8794, 2021.

Alexey Dosovitskiy, Lucas Beyer, Alexander Kolesnikov, Dirk Weissenborn, Xiaohua Zhai, Thomas Unterthiner, Mostafa Dehghani, Matthias Minderer, Georg Heigold, Sylvain Gelly, Jakob Uszkoreit, and Neil Houlsby. An image is worth 16x16 words: Transformers for image recognition at scale. In *International Conference on Learning Representations*, 2021.

Patrick Esser, Sumith Kulal, Andreas Blattmann, Rahim Entezari, Jonas Müller, Harry Saini, Yam Levi, Dominik Lorenz, Axel Sauer, Frederic Boesel, Dustin Podell, Tim Dockhorn, Zion English, and Robin Rombach. Scaling rectified flow transformers for high-resolution image synthesis. In *Forty-first International Conference on Machine Learning*, 2024.

Ying Fan, Olivia Watkins, Yuqing Du, Hao Liu, Moonkyung Ryu, Craig Boutilier, Pieter Abbeel, Mohammad Ghavamzadeh, Kangwook Lee, and Kimin Lee. Dpok: Reinforcement learning for fine-tuning text-to-image diffusion models. *Advances in Neural Information Processing Systems*, 36:79858–79885, 2023.

Zhenghan Fang, Sam Buchanan, and Jeremias Sulam. What’s in a prior? learned proximal networks for inverse problems. In *The Twelfth International Conference on Learning Representations*, 2024.

Zhenghan Fang, Mateo Díaz, Sam Buchanan, and Jeremias Sulam. Beyond scores: Proximal diffusion models. *arXiv preprint arXiv:2507.08956*, 2025.

Leander Girrbach, Stephan Alaniz, Genevieve Smith, Trevor Darrell, and Zeynep Akata. Person-centric annotations of laion-400m: Auditing bias and its transfer to models. *arXiv preprint arXiv:2510.03721*, 2025.

Jonathan Ho and Tim Salimans. Classifier-free diffusion guidance. In *NeurIPS 2021 Workshop on Deep Generative Models and Downstream Applications*, 2021.

Jonathan Ho and Tim Salimans. Classifier-free diffusion guidance, 2022.

Jonathan Ho, Ajay Jain, and Pieter Abbeel. Denoising diffusion probabilistic models. In *Advances in Neural Information Processing Systems (NeurIPS)*, 2020.

Peter Holderrieth, Uriel Singer, Tommi Jaakkola, Ricky T. Q. Chen, Yaron Lipman, and Brian Karrer. Glass flows: Transition sampling for alignment of flow and diffusion models, 2025.

Zijing Hu, Fengda Zhang, Long Chen, Kun Kuang, Jiahui Li, Kaifeng Gao, Jun Xiao, Xin Wang, and Wenwu Zhu. Towards better alignment: Training diffusion models with reinforcement learning against sparse rewards. In *Proceedings of the Computer Vision and Pattern Recognition Conference*, pages 23604–23614, 2025.

Xuan Ju, Ailing Zeng, Jianan Wang, Qiang Xu, and Lei Zhang. Human-art: A versatile human-centric dataset bridging natural and artificial scenes. In *Proceedings of the IEEE/CVF conference on computer vision and pattern recognition*, pages 618–629, 2023.

Tero Karras, Miika Aittala, Timo Aila, and Samuli Laine. Elucidating the design space of diffusion-based generative models. *Advances in neural information processing systems*, 35:26565–26577, 2022.

Diederik P. Kingma and Max Welling. Auto-Encoding Variational Bayes. In *2nd International Conference on Learning Representations, ICLR 2014, Banff, AB, Canada, April 14-16, 2014, Conference Track Proceedings*, 2014.

Yuval Kirstain, Adam Polyak, Uriel Singer, Shahbuland Matiana, Joe Penna, and Omer Levy. Pick-a-pic: An open dataset of user preferences for text-to-image generation. *Advances in neural information processing systems*, 36:36652–36663, 2023.

Shikai Li, Jianglin Fu, Kaiyuan Liu, Wentao Wang, Kwan-Yee Lin, and Wayne Wu. Cosmicman: A text-to-image foundation model for humans. In *Proceedings of the IEEE/CVF Conference on Computer Vision and Pattern Recognition*, pages 6955–6965, 2024.

Zhenyi Liao, Qingsong Xie, Chen Chen, Hannan Lu, and Zhijie Deng. Facescore: Benchmarking and enhancing face quality in human generation. *arXiv preprint arXiv:2406.17100*, 2024.

Yaron Lipman, Ricky TQ Chen, Heli Ben-Hamu, Maximilian Nickel, and Matthew Le. Flow matching for generative modeling. *arXiv preprint arXiv:2210.02747*, 2022.

Jie Liu, Gongye Liu, Jiajun Liang, Yangguang Li, Jiaheng Liu, Xintao Wang, Pengfei Wan, Di Zhang, and Wanli Ouyang. Flow-grpo: Training flow matching models via online rl. *arXiv preprint arXiv:2505.05470*, 2025.

Xingchao Liu, Chengyue Gong, and qiang liu. Flow straight and fast: Learning to generate and transfer data with rectified flow. In *The Eleventh International Conference on Learning Representations*, 2023.

Cheng Lu, Yuhao Zhou, Fan Bao, Jianfei Chen, Chongxuan Li, and Jun Zhu. Dpm-solver: A fast ode solver for diffusion probabilistic model sampling in around 10 steps. *Advances in neural information processing systems*, 35:5775–5787, 2022.

Cheng Lu, Yuhao Zhou, Fan Bao, Jianfei Chen, Chongxuan Li, and Jun Zhu. Dpm-solver++: Fast solver for guided sampling of diffusion probabilistic models. *Machine Intelligence Research*, pages 1–22, 2025.

Eric Luhman and Troy Luhman. Knowledge distillation in iterative generative models for improved sampling speed. *arXiv preprint arXiv:2101.02388*, 2021.

Alex Nichol, Prafulla Dhariwal, Aditya Ramesh, Pranav Shyam, Pamela Mishkin, Bob McGrew, Ilya Sutskever, and Mark Chen. Glide: Towards photorealistic image generation and editing with text-guided diffusion models. In *International Conference on Machine Learning*, 2021.

Bernt Oksendal. *Stochastic differential equations: an introduction with applications*. Springer Science & Business Media, 2013.

Dustin Podell, Zion English, Kyle Lacey, Andreas Blattmann, Tim Dockhorn, Jonas Müller, Joe Penna, and Robin Rombach. SDXL: Improving latent diffusion models for high-resolution image synthesis. In *The Twelfth International Conference on Learning Representations*, 2024.

Qwen, ., An Yang, Baosong Yang, Beichen Zhang, Binyuan Hui, Bo Zheng, Bowen Yu, Chengyuan Li, Dayiheng Liu, Fei Huang, Haoran Wei, Huan Lin, Jian Yang, Jianhong Tu, Jianwei Zhang, Jianxin Yang, Jiaxi Yang, Jingren Zhou, Junyang Lin, Kai Dang, Keming Lu, Keqin Bao, Kexin Yang, Le Yu, Mei Li, Mingfeng Xue, Pei Zhang, Qin Zhu, Rui Men, Runji Lin, Tianhao Li, Tianyi Tang, Tingyu Xia, Xingzhang Ren, Xuancheng Ren, Yang Fan, Yang Su, Yichang Zhang, Yu Wan, Yuqiong Liu, Zeyu Cui, Zhenru Zhang, and Zihan Qiu. Qwen2.5 technical report, 2025.

Colin Raffel, Noam Shazeer, Adam Roberts, Katherine Lee, Sharan Narang, Michael Matena, Yanqi Zhou, Wei Li, and Peter J Liu. Exploring the limits of transfer learning with a unified text-to-text transformer. *Journal of machine learning research*, 21(140):1–67, 2020.

Aditya Ramesh, Mikhail Pavlov, Gabriel Goh, Scott Gray, Chelsea Voss, Alec Radford, Mark Chen, and Ilya Sutskever. Hierarchical text-conditional image generation with clip latents. *arXiv preprint arXiv:2204.06125*, 2022.

Robin Rombach, Andreas Blattmann, Dominik Lorenz, Patrick Esser, and Björn Ommer. High-resolution image synthesis with latent diffusion models. In *IEEE Conference on Computer Vision and Pattern Recognition (CVPR)*, 2022.

Chitwan Saharia, William Chan, Saurabh Saxena, Lala Li, Jay Whang, Emily Denton, Seyed Kamyar Ghasemipour, Raphael Lopes, and et al. Photorealistic text-to-image diffusion models with deep language understanding. In *Advances in Neural Information Processing Systems (NeurIPS)*, 2022.

Tim Salimans and Jonathan Ho. Progressive distillation for fast sampling of diffusion models. In *International Conference on Learning Representations (ICLR)*, 2022.

Christoph Schuhmann. LAION-Aesthetics. <https://laion.ai/blog/laion-aesthetics/>, 2022. Accessed: 2025-11-08.

John Schulman, Sergey Levine, Pieter Abbeel, Michael Jordan, and Philipp Moritz. Trust region policy optimization. In *Proceedings of the 32nd International Conference on Machine Learning*, pages 1889–1897, Lille, France, 2015. PMLR.

John Schulman, Filip Wolski, Prafulla Dhariwal, Alec Radford, and Oleg Klimov. Proximal policy optimization algorithms, 2017.

Zhihong Shao, Peiyi Wang, Qihao Zhu, Runxin Xu, Junxiao Song, Xiao Bi, Haowei Zhang, Mingchuan Zhang, YK Li, Yang Wu, et al. Deepseekmath: Pushing the limits of mathematical reasoning in open language models. *arXiv preprint arXiv:2402.03300*, 2024.

Jascha Sohl-Dickstein, Eric Weiss, Niru Maheswaranathan, and Surya Ganguli. Deep unsupervised learning using nonequilibrium thermodynamics. In *International conference on machine learning*, pages 2256–2265. pmlr, 2015.

Jiaming Song, Chenlin Meng, and Stefano Ermon. Denoising diffusion implicit models. In *International Conference on Learning Representations*, 2021a.

Yang Song and Stefano Ermon. Generative modeling by estimating gradients of the data distribution. *Advances in neural information processing systems*, 32, 2019.

Yang Song, Jascha Sohl-Dickstein, Diederik P. Kingma, Abhishek Kumar, Stefano Ermon, and Ben Poole. Score-based generative modeling through stochastic differential equations. In *International Conference on Learning Representations (ICLR)*, 2021b.

Masatoshi Uehara, Yulai Zhao, Tommaso Biancalani, and Sergey Levine. Understanding reinforcement learning-based fine-tuning of diffusion models: A tutorial and review. *arXiv preprint arXiv:2407.13734*, 2024a.

Masatoshi Uehara, Yulai Zhao, Kevin Black, Ehsan Hajiramezanali, Gabriele Scalia, Nathaniel Lee Diamant, Alex M Tseng, Tommaso Biancalani, and Sergey Levine. Fine-tuning of continuous-time diffusion models as entropy-regularized control. *arXiv preprint arXiv:2402.15194*, 2024b.

Xiaoshi Wu, Yiming Hao, Keqiang Sun, Yixiong Chen, Feng Zhu, Rui Zhao, and Hongsheng Li. Human preference score v2: A solid benchmark for evaluating human preferences of text-to-image synthesis. *arXiv preprint arXiv:2306.09341*, 2023.

Yuchen Wu, Yuxin Chen, and Yuting Wei. Stochastic runge-kutta methods: Provable acceleration of diffusion models. *arXiv preprint arXiv:2410.04760*, 2024.

Weihao Xia, Yujiu Yang, Jing-Hao Xue, and Baoyuan Wu. Tedigan: Text-guided diverse face image generation and manipulation. In *IEEE Conference on Computer Vision and Pattern Recognition (CVPR)*, 2021a.

Weihao Xia, Yujiu Yang, Jing-Hao Xue, and Baoyuan Wu. Towards open-world text-guided face image generation and manipulation. *arxiv preprint arxiv: 2104.08910*, 2021b.

Hu Xu, Saining Xie, Xiaoqing Ellen Tan, Po-Yao Huang, Russell Howes, Vasu Sharma, Shang-Wen Li, Gargi Ghosh, Luke Zettlemoyer, and Christoph Feichtenhofer. Demystifying clip data. *arXiv preprint arXiv:2309.16671*, 2023a.

Jiazheng Xu, Xiao Liu, Yuchen Wu, Yuxuan Tong, Qinkai Li, Ming Ding, Jie Tang, and Yuxiao Dong. Imagereward: Learning and evaluating human preferences for text-to-image generation. *Advances in Neural Information Processing Systems*, 36:15903–15935, 2023b.

Zeyue Xue, Jie Wu, Yu Gao, Fangyuan Kong, Lingting Zhu, Mengzhao Chen, Zhiheng Liu, Wei Liu, Qiushan Guo, Weilin Huang, et al. Dancegrpo: Unleashing grpo on visual generation. *arXiv preprint arXiv:2505.07818*, 2025.

Qinsheng Zhang and Yongxin Chen. Fast sampling of diffusion models with exponential integrator. In *The Eleventh International Conference on Learning Representations*, 2023.

A Full definition of the GRPO objective

The full GRPO objective used in our work is defined as:

$$\mathcal{J}_{\text{GRPO}}(\theta) = \sum_{i=1}^G \sum_{k=1}^K \left\{ R_k^{(i)}(\theta) - \beta_{\text{KL}} D_{\text{KL},k}^{(i)}(\theta) \right\},$$

where

$$R_k^{(i)}(\theta) = \min \left[r_k^{(i)}(\theta) \hat{A}^{(i)}, \text{clip} \left(r_k^{(i)}(\theta), 1 - \epsilon, 1 + \epsilon \right) \hat{A}^{(i)} \right],$$

and

$$r_k^{(i)}(\theta) = \frac{p_{\theta}(X_{k-1}^{(i)} | X_k^{(i)}, c)}{p_{\theta_{\text{old}}}(X_{k-1}^{(i)} | X_k^{(i)}, c)}.$$

This clipped reward imposes a trust-region-like constraint to avoid large policy updates and stabilizes training under noisy reward estimates (Schulman et al., 2015, 2017).

B Processing Details of the LAION-Face-T2I-15M Dataset

We start from the LAION-Face dataset⁶ and apply additional filtering to retain images with a minimum short edge of ≥ 256 pixels, aspect ratio in $[9/16, 16/9]$, and an aesthetic score ≥ 4.5 (the LAION aesthetic predictor (Schuhmann, 2022)), resulting in a high-resolution and high-quality collection of roughly 15M images.

Since the raw LAION-Face captions are limited in details and not suitable for fine-grained text-to-image training, we recaption all images using the Qwen-2.5-7B vision-language model (Qwen et al., 2025) with the following prompt:

Write a concise summary of the image in 30 words. Describe the main subjects, actions, and any noticeable details such as face, hair, clothes, ethnicity, or background.
Describe the image style, such as photography, painting, or cartoon. The description should be a suitable image generation prompt.

This process yields high-quality captions suitable for training human text-to-image models from scratch.

In addition to the base dataset, we also construct LAION-Face-Hand-3M, a subset of LAION-Face-T2I-15M tailored for hand image generation. We employ Qwen-2.5-7B to identify images containing close-up views of hands and generate detailed captions describing the hand attributes, with the prompt shown below:

Does this image meet **all** of the following criteria?
1. It is a **real photograph**, not a drawing or digital rendering.
2. It shows a **close-up view** of the upper body (head to waist).
3. There is a **single person** in the image.
4. At least **one hand** is clearly visible and engaged in a motion or gesture (e.g., pointing, holding, touching, etc.).

If yes, respond with 'Yes' and on a new line, a caption of the image in about 30 words.
Describe the hands in detail, covering:

⁶<https://github.com/FacePerceiver/LAION-Face>

- Number of hands visible (e.g., 'one hand', 'both hands')
- Position relative to the body (e.g., 'resting on lap', 'raised near face')
- Finger gesture or configuration (e.g., 'fingers curled', 'spread apart', 'pointing')
- Activity or interaction if any (e.g., 'adjusting clothing', 'touching chin', 'gesturing toward camera')
- Visibility quality (e.g., 'clearly visible', 'partially obscured').

If no, respond with 'No' and nothing else.

The resulting captions describe the number of hands, their position relative to the body, finger gestures, interactions (e.g., holding objects or touching the face), and visibility quality. This level of annotation provides training data with a much finer level of supervision for learning human-hand generation, an area where current models often fail.



A young girl with blonde pigtails, wearing a floral dress, stands in a field of wildflowers. She smiles softly, looking directly at the camera. The background is blurred with golden hues, suggesting a sunset. The image has a natural, candid feel.



A man stands confidently in an orange hoodie with a small logo on the chest. He has short dark hair and a neutral expression. The background is plain white, emphasizing the subject. The image appears to be a professional photograph.



A woman with long dark hair and a serious expression holds an orange flower near her mouth. She wears a luxurious fur coat. The background is blurred, suggesting a formal setting. The image appears to be a photograph.



Three cyclists in black gear and orange helmets ride through a grassy area marked by yellow tape. One cyclist in the foreground has a bald head and wears a red helmet. The background features trees and a large industrial structure. The image is a realistic photograph.

Figure 5: Example images and corresponding fine-grained captions in the LAION-Face-T2I-15M dataset.

C Experimental Details

Implementation. To enable efficient sampling of high-resolution images, we perform generation in the latent space of a pretrained variational autoencoder (VAE) (Kingma and Welling, 2014; Rombach et al., 2022), which compresses images into a lower-dimensional representation. Specifically, we use the VAE from Stable Diffusion 3.5 (Esser et al., 2024), which encodes an image of size $H \times W \times 3$ to a latent dimension of $H/8 \times W/8 \times 16$.

For textual conditioning, we leverage a combination of pretrained text encoders to extract semantically rich and diverse representations of the input prompt. In particular, we use the Meta-CLIP encoder (Xu et al., 2023a) trained on openly curated data and the T5 encoder (Raffel et al., 2020), which has been observed to benefit generation for complex prompts involving dense details (Esser et al., 2024), aligning well with our objective of fine-grained human image generation. The outputs from the two encoders are combined by padding to a common embedding dimension and then concatenating along the token axis.

For the proximal network $f_\theta(x; t, \lambda, c)$, we adopt the U-ViT architecture (Bao et al., 2023)—a Vision Transformer (ViT) (Dosovitskiy et al., 2021) based backbone—for its flexibility in handling variation in the input space by treating all inputs as tokens. This network design naturally accommodates the additional λ -conditioning present in the proximal model but absent in conventional

score networks. The joint distribution of (t, λ) during training is defined according to the proximal operators required for a range of potential sampling steps ($\{4, 5, 6, 7, 8, 9, 10, 25\}$), to target efficient sampling. This conditional proximal diffusion model serves as the foundation for the reinforcement learning stage described next.

Training. Our models are trained from scratch on 256^2 images and their corresponding captions from LAION-FACE-T2I-15M. We train a score-based and a proximal diffusion model, both using a batch size of 2,048 and for 100 thousand steps. We train ProxT2I using proximal matching loss, with a learning rate of 8×10^{-5} . We set $\zeta = 1.0$ in the proximal matching loss, and sample (t, λ) according to the discretization schemes corresponding to the sampling steps: $\{4, 5, 6, 7, 8, 9, 10, 25\}$. The score models are trained using the score matching loss (Song and Ermon, 2019; Ho et al., 2020) with a learning rate of 4×10^{-4} following (Bao et al., 2023). We randomly set the input text conditioning to an empty string with a probability $p_\emptyset = 0.1$ to train unconditional models for classifier-free guidance for both score and proximal models.

We then optimize the pretrained models for specific rewards using reinforcement learning with GRPO. We use PickScore (Kirstain et al., 2023) as the reward model and a training dataset contains 3,000 prompts. We draw samples using 10 sampling steps. We set the weight for the KL regularization to $\beta = 0.001$. We set the group size to $G = 24$ and the number of sampling steps to $K = 10$. Each training batch contains 12 prompts. We use a gradient accumulation of 6 batches, and train each model for 1,000 steps.

To study the performance of ProxT2I for higher-resolution generation, we finetune the pretrained 256^2 models on 512^2 images from LAION-FACE-T2I-15M and LAION-FACE-T2I-HAND-3M. We also include images from MMCelebA-HQ (Xia et al., 2021a) and CosmicMan (Li et al., 2024) to improve training data diversity, with captions generated following the same procedures as LAION-FACE-T2I-15M for all images. Images are filtered by short edge ≥ 512 and aspect ratio in $[0.9, 1/0.9]$. This stage uses a batch size of 256 and trains both score and ProxT2I for 60k steps, with a learning rate of 1×10^{-5} . Finally, both the score and proximal models are fine-tuned using GRPO on 100 curated prompts with PickScore as the reward model for 1,000 steps, with other settings the same as the 256^2 experiment.

D Additional Results



(a) 6 sampling steps.

(b) 10 sampling steps.

Figure 6: Qualitative comparison of generated images at 256^2 resolution with 6 and 10 sampling steps.

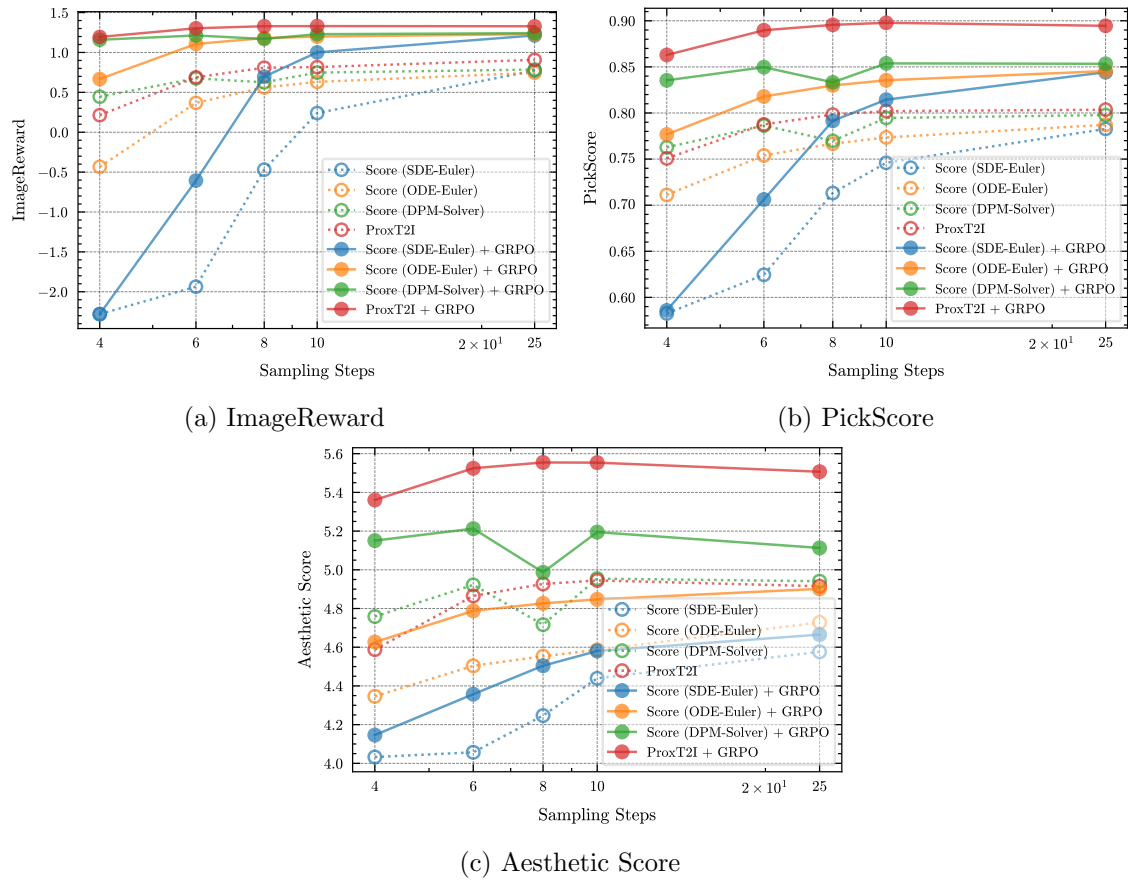


Figure 7: Comparison of additional metrics at 256^2 resolution.

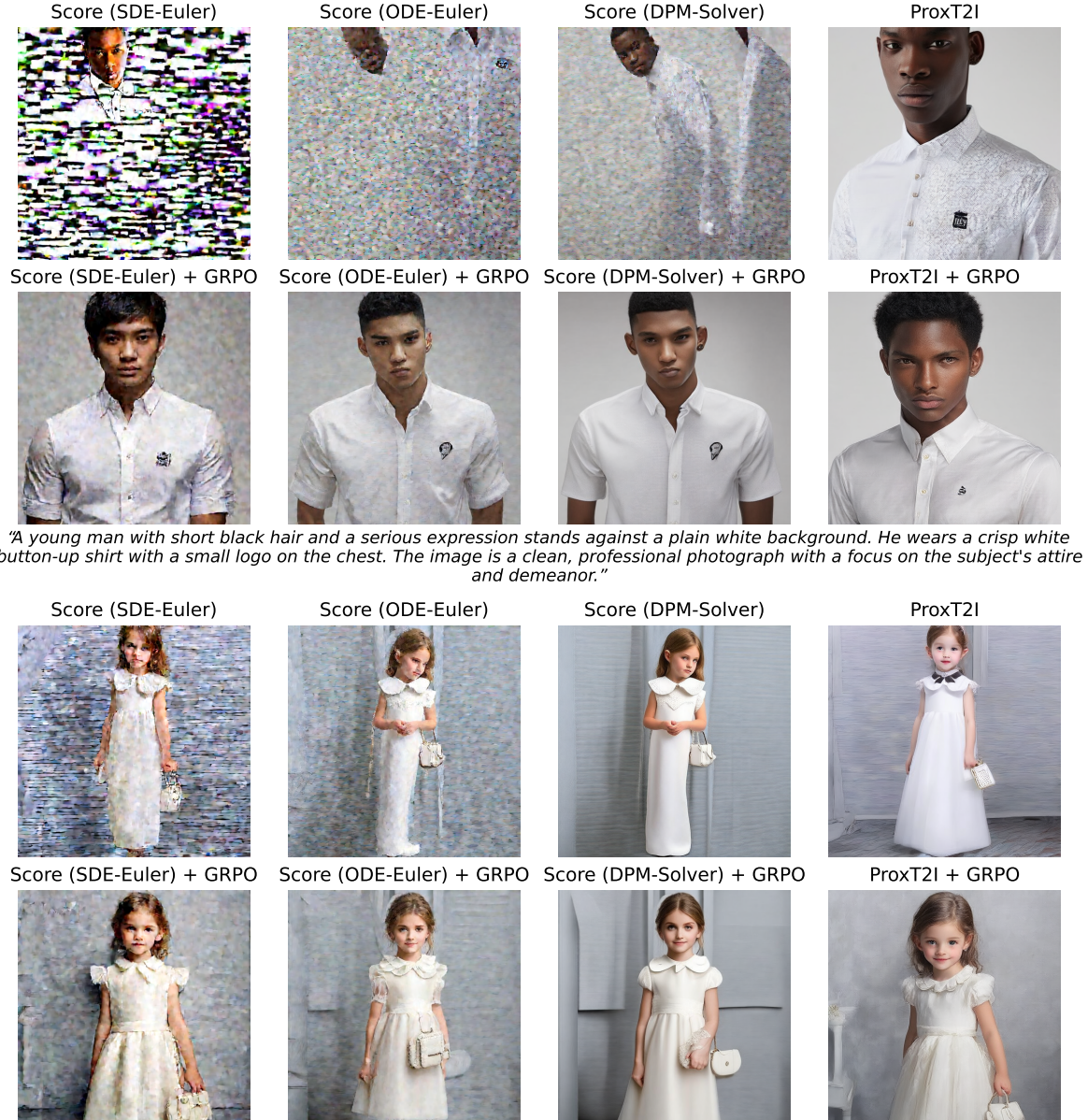


Figure 8: Qualitative comparison of 512^2 generations at 10 sampling steps.

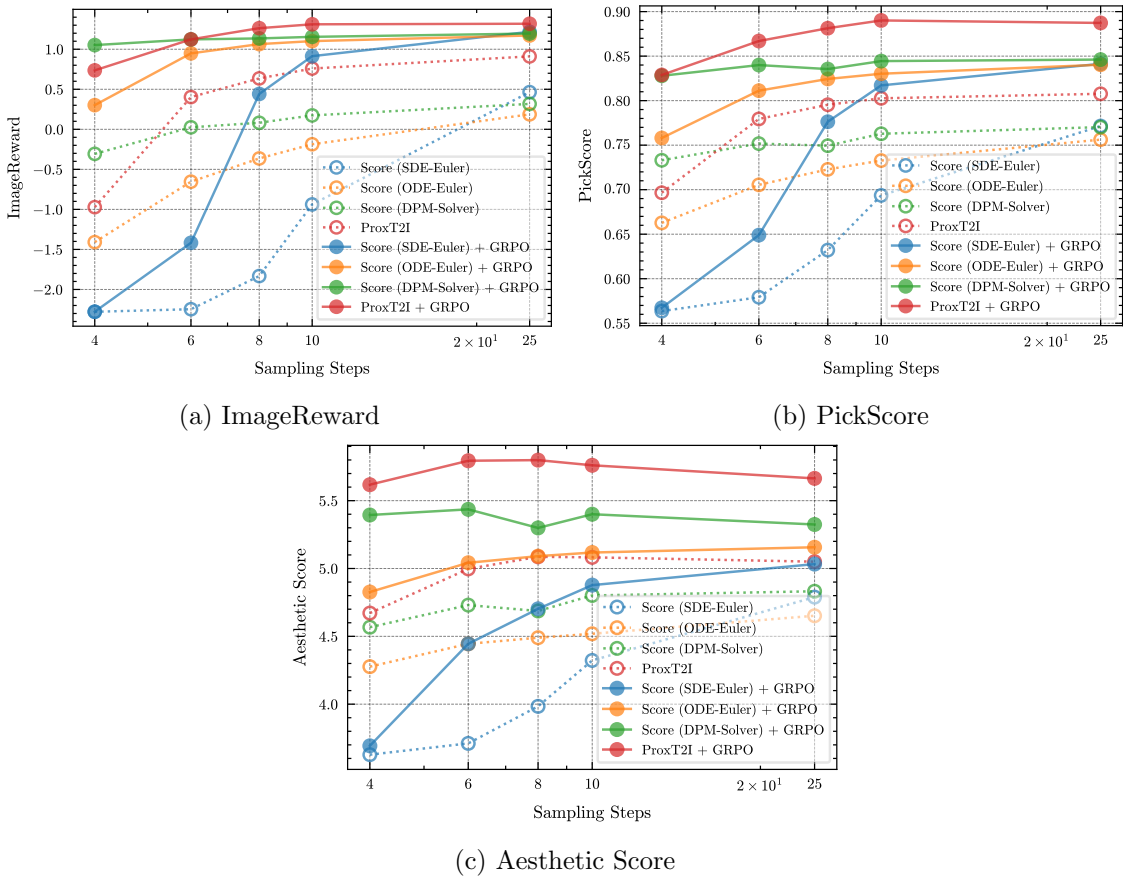


Figure 9: Comparison of additional metrics at 512^2 resolution.

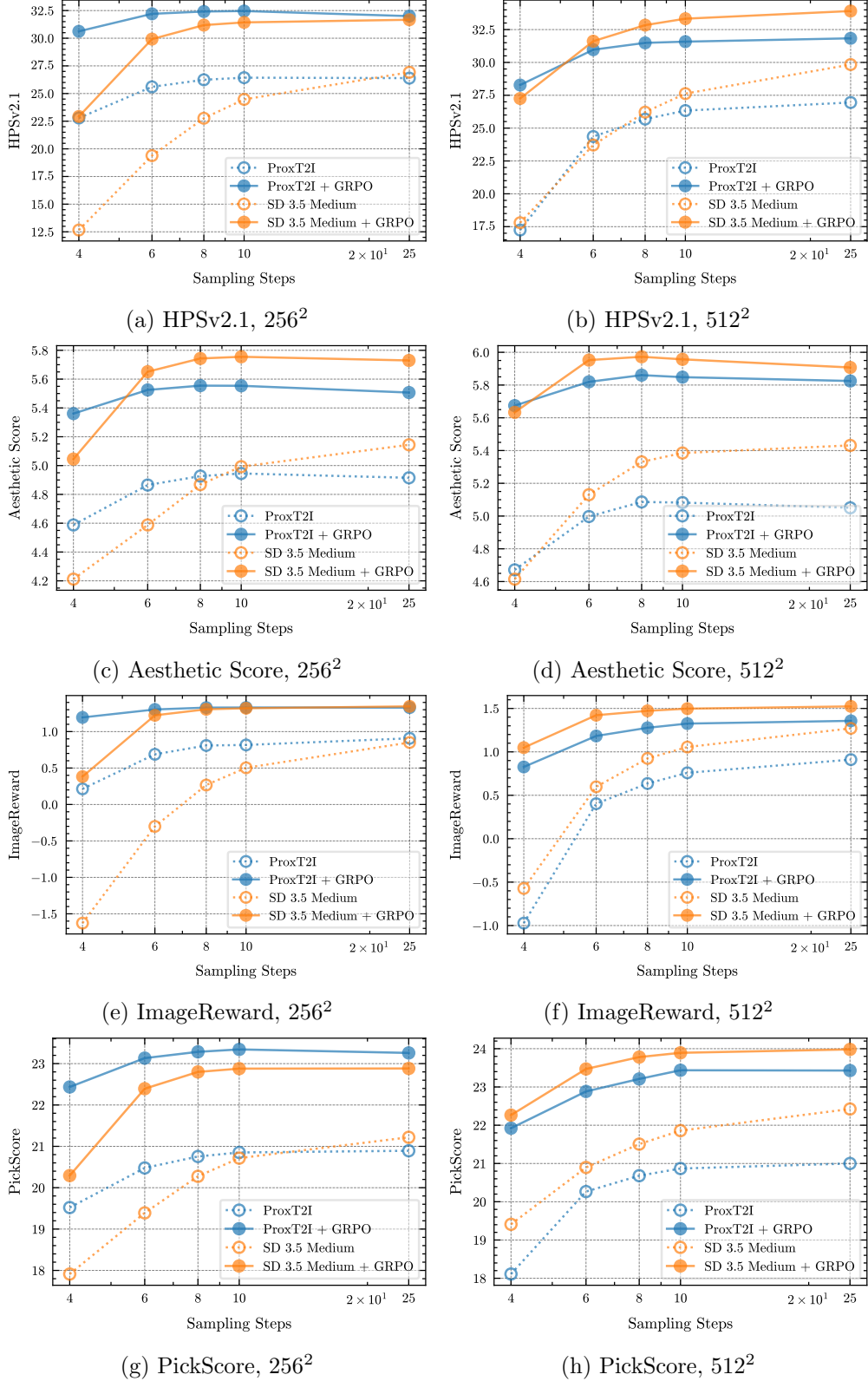


Figure 10: Comparison with StableDiffusion (SD) 3.5 Medium (Esser et al., 2024) and its RL finetuned model from FlowGRPO (Liu et al., 2025) at 256² and 512² resolutions.

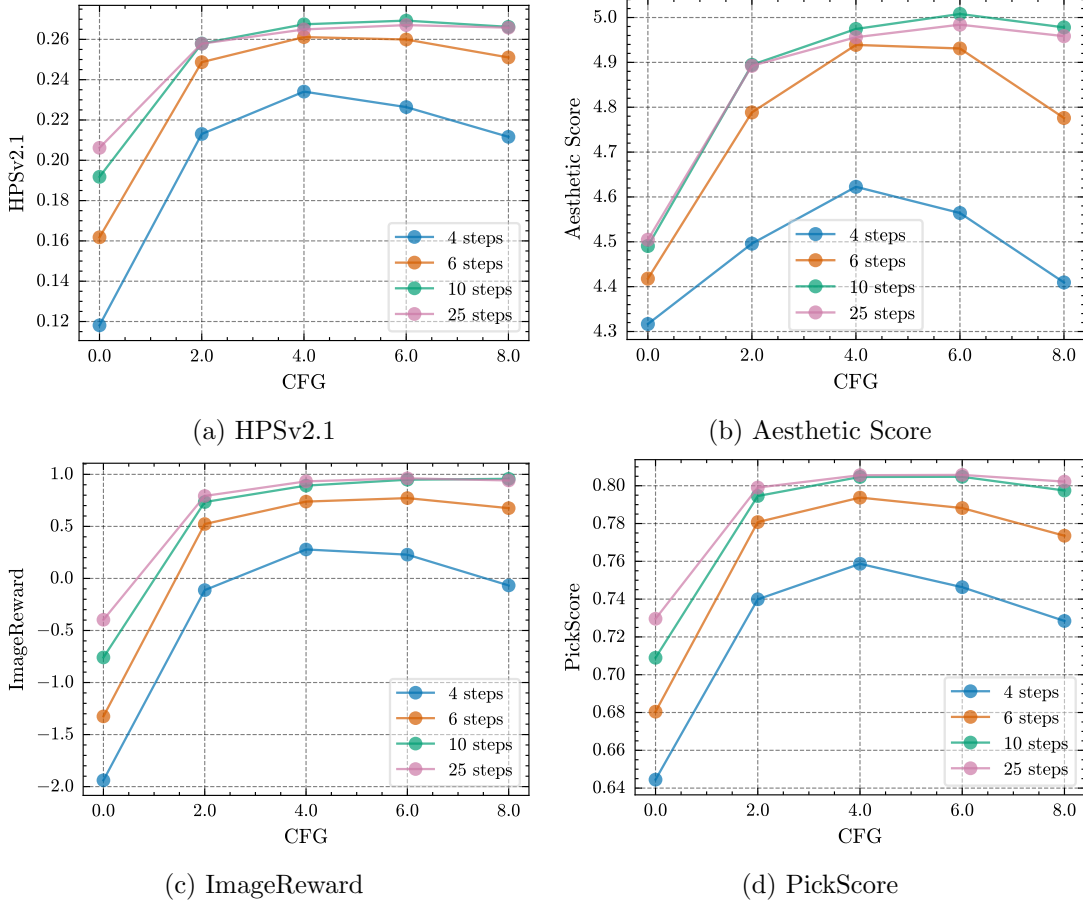


Figure 11: Effect of CFG level ω for ProxT2I at different sampling step numbers. Here, CFG=0 corresponds to using no guidance, i.e., using only the conditional proximal operator without the unconditional one.



"Two soccer players in bright yellow Brazil training jerseys stand on a green field, engaged in conversation. One has short dark hair, while the other has a shaved head. The jerseys feature logos and text. The image is a realistic photograph."



"A newborn baby with light skin and dark hair is sleeping peacefully on a soft pink blanket. The baby wears a delicate pink headband with a large flower. The image is a realistic photograph with soft lighting and gentle colors."

Figure 12: Effect of CFG level ω on ProxT2I-generated images (256^2 resolution and 10 sampling steps). Increasing CFG level from 0 improves image quality and text-image alignment, while overly large values yield degraded result.

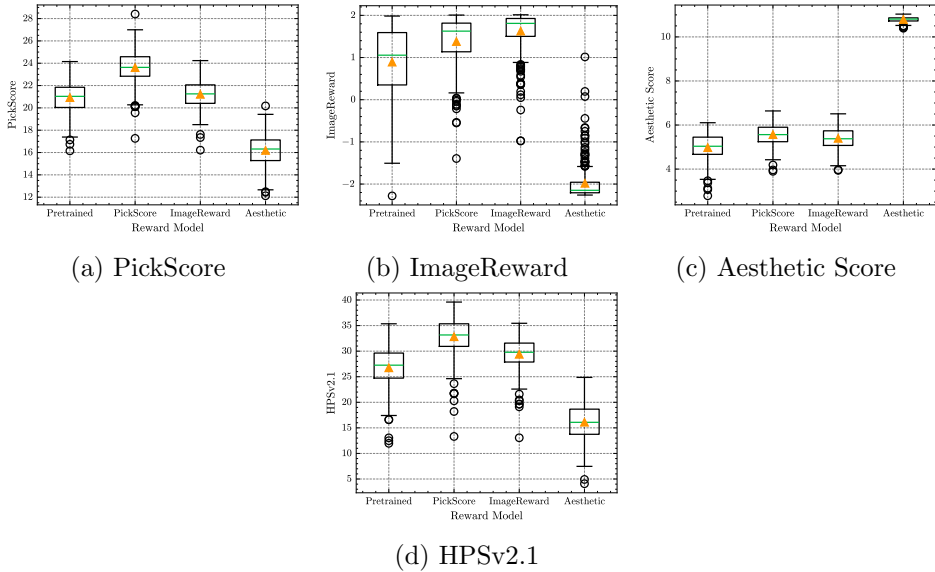


Figure 13: Comparison of ProxT2I models finetuned with different reward functions. We apply reinforcement learning (RL) using three reward models: PickScore, ImageReward, and Aesthetic Score, and compare them with the pretrained (non-RL) baseline. Each panel shows the results of all models for a specific evaluation metric. Besides the three training rewards, we include HPSv2.1, an external metric not used in RL, to assess generalization. Results are summarized over 256 testing prompts and the yellow triangle denotes the mean. All results are obtained with 10 sampling steps at 256^2 resolution.



Figure 14: Visualization of mode collapse from training ProxT2I using reinforcement learning with Aesthetic score reward. Each row shows the images generated from a different prompt. Each column shows the images generated at different checkpoints throughout training, with the first representing the model before RL finetuning. As shown, although the RL algorithm initially improves the aesthetic quality, the outputs eventually collapse, converging to nearly identical images for different prompts.